A Simplified Cerebellum-Based Model for Motor Control in Brain Based Devices

Vui Ann Shim, Chris Stephen Naveen Ranjit, Bo Tian, and Huajin Tang

Institute for Infocomm Research, 1 Fusionopolis Way,
#21-01 Connexis, 138632, Singapore
{shimva,btian,htang}@i2r.a-star.edu.sg, ranjitcsn@gmail.com

Abstract. The cerebellar system is implicated in motor learning for movement coordination. In this paper, we suggest a simplified cerebellar model with priority-based delayed eligibility trace learning rule (S-CDE) that enables a mobile agent to randomly navigate in an environment. The depth information from a simulated laser sensor is encoded as neuronal region activity for velocity and turn rate control. A priority-based delayed eligibility trace learning rule is proposed to maximize the usage of input signals for learning in synapses on Purkinje cell and cells in the deep cerebellar nuclei. Asymmetric weighted sum and velocity signal conversion algorithms are designed to facilitate training in an environment containing turns of varying curvatures. S-CDE is developed as a brain-based device and tested on a simulated mobile agent which had to randomly navigate maps of Singapore and Hong Kong expressways.

Keywords: Brain-based devices, cerebellum, priority-based delayed eligibility trace learning rule, error signals, motor control.

1 Introduction

The study of the cerebellum in neuroscience, physiology, and neuroimaging has resulted in several consistent findings that implicates the cerebellar system in motor learning [1,2,3]. Error signal, the difference between reference and actual movement coordinations, has been proposed to regulate learning in the cerebellar system through synaptic eligibility traces [4]. The error signals are transmitted from the inferior olive (IO) to cerebellar regions via climbing fibers [5,6].

Inspired by the above findings, McKinstry *et al.* [7] proposed a cerebellar-based computational model with delayed eligibility trace learning rule (CDE) that learns to predict corrective motor control actions based on the experiences of reflex responses. CDE is developed as a brain-based device (BBD) [8], which is a famous platform to construct a computational model of neuroscience by incorporating features of neuroanatomy and neurophysiology of vertebrates. Visual input from a color camera is preprocessed in the middle temporal visual area (MT). Important visual features are extracted and used to trigger associations between visual cues and proper motor controls. They also suggested a delayed eligibility trace rule to govern the plasticity of synapses onto Purkinje cell (PC)

M. Lee et al. (Eds.): ICONIP 2013, Part I, LNCS 8226, pp. 520–527, 2013.

and deep cerebellar nuclei (DCN). This training rule is used to learn proper motor responses, given certain visual cues, such that error signals are avoided. The error signals are generated using input from infrared sensors, to govern the learning in PC and DCN. A laser range finder is used to detect collisions and initiate collision avoidance behavior. The results demonstrated a smooth traversal of curved paths, with each path comprised of nearly identical turn curvatures.

However, CDE suffers from several limitations. First, the complexity of CDE, which consists of 28 neural areas, 27,688 neurons, about 1.6 million synaptic connections, and three input modalities may limit its practicality in real machines. Second, CDE is inept at effective motor learning in environments with varied turn curvatures due to its limited utilization of synaptic inputs for learning. Consequently, this leads to a predicted third limitation, that is the dependence on error signals to support learned predictive motor control signals even after training for decent traversal of environments with varied turn curvatures. Lastly, there is a limit to the volatility of input stimuli, beyond which learning becomes impaired. This limitation is caused by an insufficient eligibility trace decay rate in the learning rule implemented in CDE.

With regard to the aforementioned limitations, we propose a simplified cerebellar model with priority-based delayed eligibility trace learning rule (S-CDE). First, we utilize a simulated laser sensor to generate environmental depth information. This is the only input modality, which dramatically reduces complexity of the model since visual processing in CDE imposes extravagant complexity on the system compared to its cerebellar portion. Second, a priority-based delayed eligibility trace learning rule is suggested to maximize the usage of input signals for synaptic learning on plastic connections to PC and DCN areas. This is done by introducing a mechanism to prematurely re-trigger eligibility traces upon encountering more salient synaptic inputs. Third, an increased eligibility trace decay rate is used to allow for increased input volatility. The proposed model is developed as a brain-based device and tested in a simulated mobile agent which had to randomly and smoothly navigate maps of the Singapore(SG Map) and Hong Kong(HK Map) expressways.

2 A Simplified Cerebellar Model for Motor Control

A simplified cerebellar model with priority-based delayed eligibility trace rule (S-CDE) is proposed. Compared to CDE, three major modifications, including a simplified system architecture, introduction of an eligibility trace re-triggering mechanism, and an increased eligibility trace decay rate, have been made.

2.1 System Architecture

The system architecture of S-CDE is presented in Fig. 1. A single vector of input from a laser sensor is the only sensory perception the S-CDE has of its environment. The laser streams are preprocessed, such that the sensory input is split into four different streams, each in an appropriate semantic format for the subregion it is being fed into. This modification eliminates the need for extensive

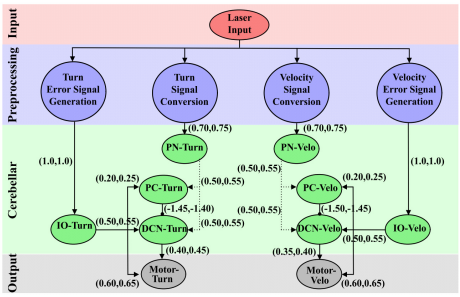

Fig. 1. System architecture of S-CDE which comprises of a sensory input layer, a pre-processing layer, a cerebellar layer, and a motor output layer. Closed arrowheads denote excitatory connections and circular endpoints denote inhibitory connections. Solid lines denote non-plastic connections while dotted lines denote plastic connections. The initial synaptic weights (c) are uniformly generated in between the maximum and minimum values as indicated near to the projections. Other settings, including learning rate (h), persistence (ω), and firing threshold (σ), are identical to the settings used in CDE [7].

processing of visual cues from a camera, thus, reducing the computational complexity. In total, the S-CDE has eight neuronal regions, 800 neuronal units, and 40,600 synaptic connections. The derivation of error signals from the laser input also eliminates the need for other input modalities. S-CDE can be divided into a sensory input layer, a pre-processing layer, a cerebellar layer, and an output motor layer. The cerebellar layer can be further divided into symmetrical *Turn* and *Velo* regions for handling turn rate and velocity computations respectively.

Sensory input is preprocessed and fed to the *PN-Turn* and *PN-Velo* areas. Error signals are derived from a subset of the sensory input and are subject to similar pre-processing before being fed to IO (*IO-Turn* and *IO-Velo*). In the cerebellar layer, PN areas(*PN-Turn* and *PN-Velo*) are linked to PC (*PC-Turn* and *PC-Velo*) and DCN (*DCN-Turn* and *DCN-Velo*) areas via plastic connections. PC controls DCN via disinhibition through its inhibitory connections, which in turn provide predictive control signals for turn rate and velocity to motor areas (*Motor-Turn* and *Motor-Velo*). Error signals from IO govern motor learning in the cerebellar regions (IO→PC and IO→DCN) and initially drive motor output in early stages of training (IO→*Motor-Turn* and IO→*Motor-Velo*).

2.2 Neuronal Responses

Standard neuronal dynamics that are implemented in BBDs are employed in S-CDE [8]. Synaptic connections can be either plastic or non-plastic and voltage-dependent or voltage-independent. In S-CDE, only voltage independent connections are used as suggested in CDE [7]. Defining j as a parent node and i as a child node, the voltage-independent connection from j to i is formulated as:

$$VI_{ij}(t) = w_{ij}s_j(t) \tag{1}$$

where w_{ij} is the synaptic weight between unit i and j, and s_j is the activation state of unit j. The activity of the neuronal areas are updated as:

$$s_i(t+1) = \phi\left(tanh\left(\sum_{j=1}^{N}(VI_{ij}(t)) + \omega s_i(t)\right)\right), \phi(x) = \begin{cases} 0; \text{ if } x < \sigma_i \\ x; \text{ otherwise} \end{cases} \quad (2)$$

where N is the number of synapses onto unit i, ω is the persistence of unit activity, and σ_i is the firing threshold of unit i.

2.3 Priority-Based Delayed Eligibility Trace Learning Rule

The synaptic strengths of the plastic connections are subject to change as follows:

$$\Delta w_{ij}(t+1) = \alpha s_i(t) \times P_j(t) \times s_i(t) \times (IO(t) - 0.02) \quad (3)$$

where α is a fixed learning rate, $P_j(t)$ is the priority eligibility trace, $s_i(t)$ is the activity of unit i and $IO(t)$ is the IO unit activity. The formulation of $P_j(t)$ is

$$P_j(t+1) = \begin{cases} 0 & \text{if } t < delay \\ s_j(t - delay) & \text{if } s_j(t - delay) \geq \epsilon \\ 0.6 \times P_j(t) & \text{otherwise} \end{cases} \quad (4)$$

where s_j is the activity of unit j, ϵ is an activity threshold and *delay* is the number of cycles offset from the current simulation cycle.

The delayed eligibility trace learning rule is used to determine the eligibility of a synapse for plasticity and if so, the amount of synaptic weight change required. The original delayed eligibility trace learning rule employed by the CDE suffers from three limitations. First, it is inept at effective motor learning in environments with varied turn curvatures. This is because once an eligibility trace over a synapse is triggered, subsequent input over that synapse is ignored for some time. Any important inputs arriving during this window is neglected, thus impairing the learning process. Second, due to the impaired learning process, the effectiveness of learned predictive motor control is limited. This would predictably create a dependence on error signals to supplement predictive motor control signals for decent traversal of such environments. Third, there is a limit to the volatility of input stimuli, beyond which learning becomes impaired. This volatility is inversely proportional to the distance between turns in a path. The input volatility limit is determined by the onset of consecutive eligibility traces during traversal of a rapid series of turns.

To overcome these limitations, a prioritized-learning concept is integrated into the learning rule. Instead of ignoring all inputs, an eligibility trace can be re-triggered if subsequent synaptic input is greater than that which triggered the initial eligibility trace. By doing so, salient inputs always have the priority for learning. Additionally, the eligibility trace decay rate has been increased from 0.9 to 0.6 to allow for a higher input volatility limit. The combined effect of the re-triggering mechanism and a higher eligibility trace decay rate is more effective predictive motor control and a higher input volatility limit, which increases learning accuracy and effectiveness when traversing relatively difficult paths.

2.4 Motor Output

Turn Rate Computation. Turn rate(°/cycle) is updated every cycle as a function of activity in the *Motor-Turn* area. Activity in the area is interpreted using population vector decoding. Each neuronal unit in *Motor-Turn* has a preferred turn-rate magnitude and direction. For explanatory purposes, neuronal units in *Motor-Turn* are indexed as t_1 to t_{100}. Units t_1 to t_{50} have a rightward preference of direction, and the preferred turn-rate magnitude of each unit grows linearly with its index. Units t_{51} to t_{100} have a leftward preference of direction, and the preferred turn-rate magnitude of each unit shrinks linearly as its index increases. To convert the activity in *Motor-Turn* to a specific turn rate, a combination of symmetric difference and population vector decoding techniques are used, expressed in equation 5(left). The resulting vector is the nett asymmetric activity in *Motor-Turn*, indexed as a_1 to a_{50}, where preferred turn-rate magnitude grows with the index, negative values indicate a leftward contribution, and positive values indicate a rightward contribution. The turn rate is calculated as shown in equation 5(right), where n is the size of $\tilde{\mathbf{a}}$ and γ is a constant defining the maximum turn rate.

$$\tilde{\mathbf{a}} = \begin{bmatrix} a_1 \\ \vdots \\ a_{50} \end{bmatrix} = \begin{bmatrix} t_1 \\ \vdots \\ t_{50} \end{bmatrix} - \begin{bmatrix} t_{100} \\ \vdots \\ t_{51} \end{bmatrix} \;;\; TurnRate = \sum_{i=1}^{n} \left\{ i \times \frac{\gamma}{100}(a_i) \right\} \tag{5}$$

Velocity Computation. Velocity(pixels/cycle) is updated every cycle as a function of activity in the *Motor-Velo* area. Activity in the area is interpreted using population vector decoding. For explanatory purposes, neuronal units in *Motor-Velo* are indexed as v_1 to v_{100}, and each has a preferred amount of braking, the magnitude of which grows linearly with its index. The conversion of activity in *Motor-Velo* to a specific velocity value is expressed in the equations below.

$$Velocity = \begin{cases} V_{max} & \text{if } \sum_{i=1}^{n} v_i = 0 \\ \| V_{max} - \beta(V_{max} - 1) \| & \text{otherwise} \end{cases} \;;\; \beta = \frac{\sum_{i=1}^{n}(i \times v_i)}{100 \sum_{j=1}^{n} v_j} \tag{6}$$

where β is a braking coefficient, a parameter that controls the amount of braking used by the agent ranging from 0 to 1, n is the size of *Motor-Velo*, v_i is the i^{th} unit of *Motor-Velo*, and V_{max} is a constant defining the maximum velocity. Through this formulation, a minimum velocity of 1 pixel/cycle is imposed.

Agent Behavior. The simulated mobile agent is given an innate behavior to move forward at a maximum speed of 6 pixels/cycle. If a collision occurs, the agent rotates in place until it is able to continue moving from its collision coordinate.

3 Results

S-CDE is developed as a brain-based model and tested in a simulated mobile agent which has to randomly and smoothly navigate SG Map and HK Map shown in Fig. 2 (a-b). Note that this simulation does not take into account physical laws such as inertia. The simulated agent is equipped with a single laser sensor and its motor capabilities are defined in terms of turn rate (°/cycle) and velocity (pixels/cycle). The simulation was executed in MATLAB on a MacBook Pro computer with a 2.66 GHz processor. One simulation cycle takes ∼25 ms.

First, experiments were conducted using SG Map to calibrate the length of the delay used in the S-CDE agent. The delays tested were 0, 3, 5 and 8 cycles. The delay resulting in the lowest motor error after 7000 simulation cycles of traversing SG Map is the calibrated delay value. Motor error for each cycle is quantified by taking the ratio of the strength of the error signal generated in the preprocessing layer to the maximum possible strength of the error signal. As a control for the experiments, a simulated agent using a reflexive motor controller was also included, which was purely driven by error signals from IO and had no predictive capabilities. This was achieved by lesioning its $DCN \rightarrow Motor$ connections. The experiments were repeated to calibrate the delay for the CDE agent, using delay values of 2, 3 and 5. The calibration of S-CDE and CDE also served as the training phase. Fig. 2 (c-d) shows a sample of S-CDE region activity during training. Following that, training effectiveness was ascertained by lesioning all connections originating from IO ($IO \rightarrow PC, IO \rightarrow DCN, IO \rightarrow Motor$) in both agents. Again, a reflexive agent was used as a control. Both SG Map and HK Map were used to evaluate training effectiveness in familiar and unfamiliar environments respectively.

Motor error output during delay calibration for both S-CDE and CDE are shown in Fig. 3 (a-b). Calibrated delays for S-CDE and CDE were determined to be 5 and 2 cycles respectively. S-CDE achieved a lower motor error rate than CDE. CDE ignores subsequent input for some time once input surpasses a threshold. If a long delay is used, CDE would only learn based on the initiation of a turn and block input arising from traversing the rest of the turn. A short

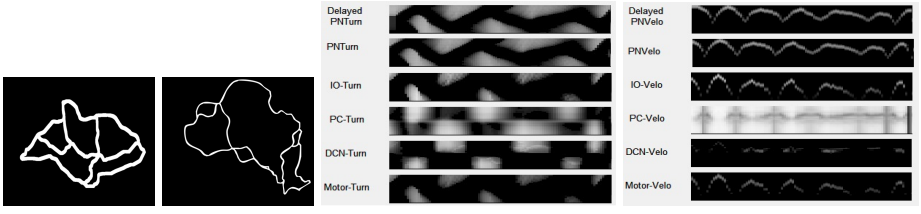

Fig. 2. (a) SG Map has a narrow average path width of 40 pixels. (b) HK map is about three times larger, and has wide average path width of 60 pixels. (c) Activity in turn-related regions during training. (d) Activity in velocity-related regions during training.

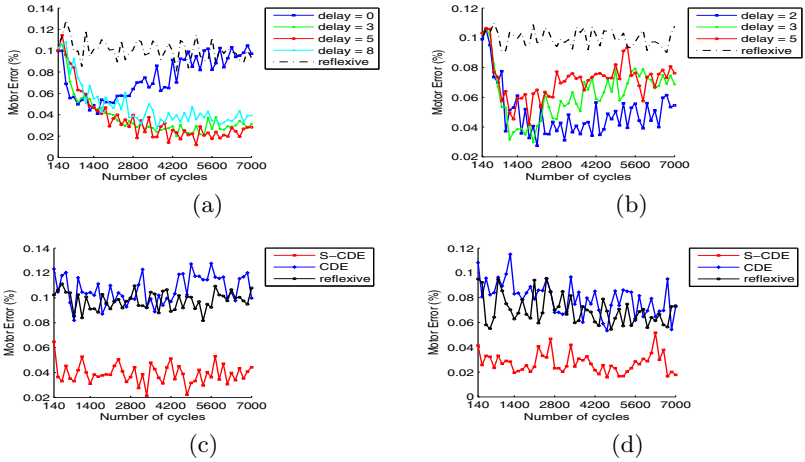

Fig. 3. Motor error during delay calibration of (a) S-CDE and (b) CDE. Motor error during training effectiveness assessment of S-CDE and CDE in (c) familiar (SG Map) and (d) unfamiliar (HK Map) environments.

enough delay would enable CDE to learn based on input from several points during the turn. However, using such a short delay severely limits the predictive capability of CDE, making it prone to higher motor error rates. S-CDE is able to base its learning on input received throughout a turn due to its re-triggering mechanism, thus resulting in lower motor error rates.

As shown in Fig. 3 (c-d), during training effectiveness evaluation, S-CDE successfully demonstrated effective predictive motor control while traversing both SG Map and HK Map despite only having prior exposure to one. CDE fails to traverse either environment satisfactorily. Due to the limited predictive capability previously mentioned, predictive motor control signals for sharp turns were generated too late to avoid impending collisions. The change in motor error rates for CDE between delay calibration and training effectiveness evaluation corroborate with the initial prediction of CDE's dependence on error signals after training for traversal of environments with varied turn curvatures. The performance of S-CDE in both maps during training effectiveness evaluation was comparable to that achieved at the end of delay calibration, which strongly suggests effective retention of learned predictive responses, and demonstrates its robustness in an unfamiliar environment.

4 Conclusion

In this paper, a simplified cerebellar model for predictive motor control has been presented. It has a simplified neural architecture due to the reduction of input modalities. It has demonstrated effective motor learning in environments with varied turn curvatures because of the introduction of the priority-based delayed eligibility trace learning rule. It is also robust while traversing new environments.

Acknowledgments. This work was supported by the Agency for Science, Technology, and Research, Singapore under SERC Grant 0921570130.

References

1. Houk, J.C., Buckingham, J.T., Barto, A.G.: Learning in and from brain-based devices. Behavioral and Brain Sciences 19(3), 368–383 (1996)
2. Llinás, R.R.: Cerebellar motor learning vs. cerebellar motor timing: The climbing fiber story. The Journal of Physiology 589(14), 3423–3432 (2011)
3. Schlerf, J., Ivry, R.B., Diedrichsen, J.: Encoding of sensory prediction errors in the human cerebellum. The Journal of Neuroscience 32(14), 4913–4922 (2012)
4. Medina, J.F., Carey, M.R., Lisberger, S.G.: The representation of time for motor learning. Neuron 45(1), 157–167 (2005)
5. Ito, M.: Error detection and representation in the olivo-cerebellar system. Frontiers in Neural Circuits 7(1), 1–8 (2013)
6. Wolpert, D.M., Miall, R.C., Kawato, M.: Internal models in the cerebellum. Trends in Cognitive Sciences 2(9), 338–347 (1998)
7. McKinstry, J.L., Edelman, G.M., Krichmar, J.L.: A cerebellar model for predictive motor control tested in a brain-based device. Proceedings of the National Academy of Sciences 103(9), 3387–3392 (2006)
8. Edelman, G.M.: Learning in and from brain-based devices.. Science 318(5853), 1103–1105 (2007)